Article n°4

Sommaire

1- Page de garde du journal mentionnant la ou les bases de son indexation ou le numéro d'identification ISSN

- **https://www.worldscientific.com/page/mplb/aims-scope**
- **https://www.worldscientific.com/page/mplb/abstracted-indexed**

2- L'abstract de l'article ou toutes informations référencées par la base de données d'indexation (preuves d'indexation)

- **https://www.scopus.com/sourceid/29055**
- **https://mathscinet.ams.org/mathscinet/search/journal/profile?groupId=3277**
- **https://zbmath.org/serials/?q=MPLB**

3- Tiré-à-part de l'article

https://doi.org/10.1142/S021798491850015X

1- Page de garde du journal mentionnant la ou les bases de son indexation ou le numéro d’identification ISSN

Modern Physics Letters B

Condensed Matter Physics; Statistical Physics; Atomic, Molecular and Optical Physics

ISSN (print): 0217-9849 | ISSN (online): 1793-6640

Aims & Scope

MPLB opens a channel for the fast circulation of important and useful research findings in Condensed Matter Physics, Statistical Physics, as well as Atomic, Molecular and Optical Physics. A strong emphasis is placed on topics of current interest, such as cold atoms and molecules, new topological materials and phases, and novel low-dimensional materials. The journal also contains a Brief Reviews section with the purpose of publishing short reports on the latest experimental findings and urgent new theoretical developments.

Modern Physics Letters B

Condensed Matter Physics; Statistical Physics; Atomic, Molecular and Optical Physics

ISSN (print): 0217-9849 | ISSN (online): 1793-6640

Tools Share

Submit an article

Subscribe

Abstracted & Indexed in

- Academic OneFile
- Academic Search Complete/ Elite/ Premier
- Astrophysics Data System (ADS) Abstract Service
- Baidu
- Chemical Abstracts Service
- CNKI Scholar
- CnpLINKer
- CrossRef
- CSA Meteorological & Geoastrophysical Abstracts
- Current Contents®/Physical, Chemical & Earth Sciences
- Ebsco Discovery Service
- Ebsco Electronic Journal Service (EJS)
- ExLibris Primo Central
- Google Scholar
- INSPEC
- ISI Alerting Services
- J-Gate
- Journal Citation Reports/Science Edition
- Materials Science Citation Index (MSCI)
- Mathematical Reviews / MathSciNet®
- Naver
- NSTL - National Science and Technology Libraries
- OCLC WorldCat®
- ProQuest SciTech Premium Collection
- Science Citation Index®
- Science Citation Index Expanded
- Scopus
- The Summon® Service
- Zentralblatt MATH

All journal articles published by World Scientific are archived at *Portico* which provides long-term preservation.

2- L’abstract de l’article ou toutes informations référencées par la base de données d’indexation (preuves d'indexation)

PREUVE D'INDEXATION DANS SCOPUS

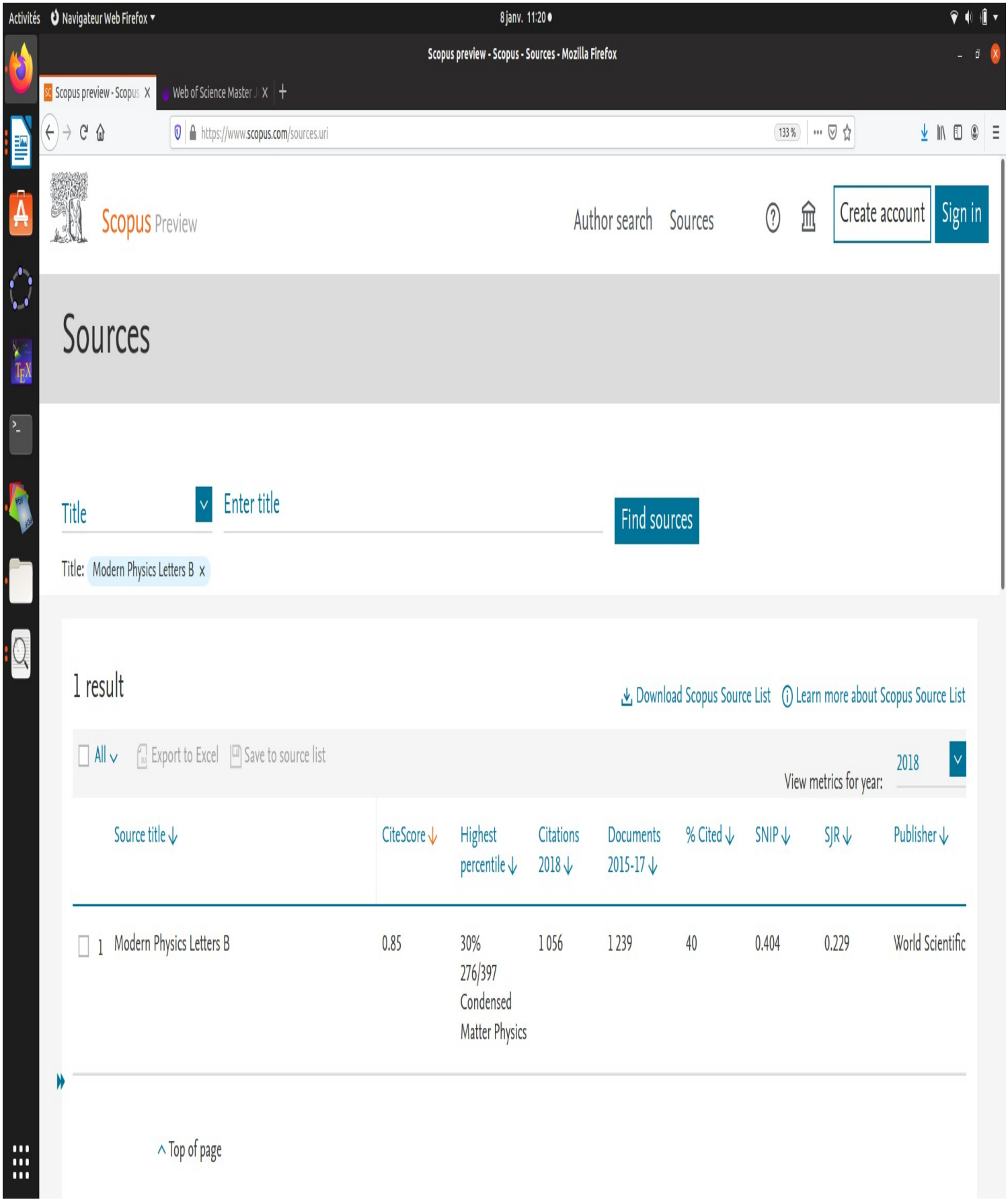
Activités
Navigateur Web Firefox
8 janv. 11:20
Scopus preview - Scopus - Sources - Mozilla Firefox
Scopus preview - Scopus
Web of Science Master
https://www.scopus.com/sources.uri
133 %
Scopus Preview
Author search
Sources
Create account
Sign in
Sources
Title
Enter title
Find sources
Title: Modern Physics Letters B x
1 result
Download Scopus Source List
Learn more about Scopus Source List
All
Export to Excel
Save to source list
View metrics for year:
2018
Source title
CiteScore
Highest percentile
Citations 2018
Documents 2015-17
% Cited
SNIP
SJR
Publisher
1 Modern Physics Letters B
0.85
30% 276/397 Condensed Matter Physics
1 056
1 239
40
0.404
0.229
World Scientific
Top of page

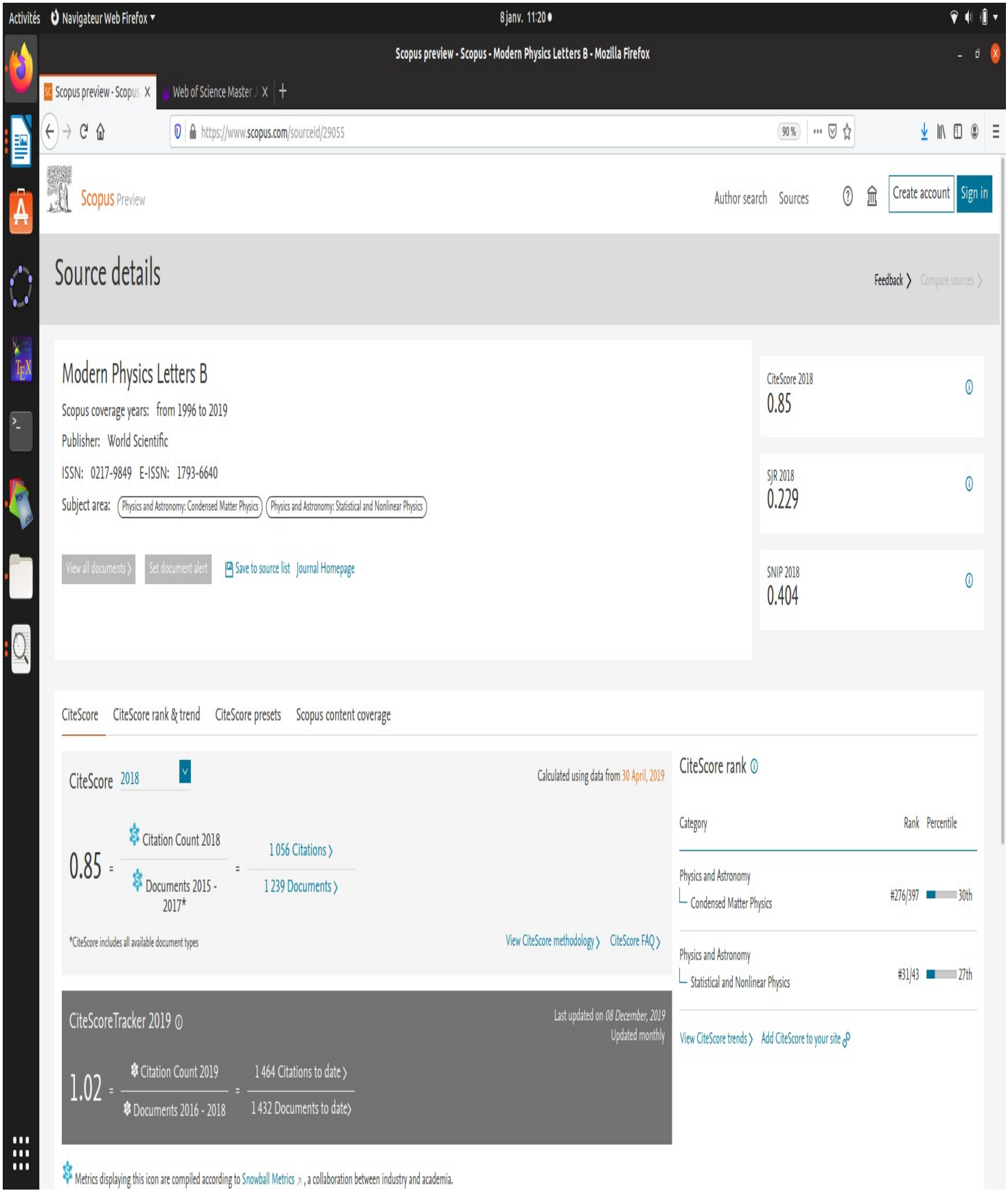
Activités
Navigateur Web Firefox
8 janv. 11:20
Scopus preview - Scopus - Modern Physics Letters B - Mozilla Firefox
Scopus preview - Scopus
Web of Science Master J
https://www.scopus.com/sourceid/29055
90 %
Scopus Preview
Author search
Sources
Create account
Sign in
Source details
Feedback
Compare sources
Modern Physics Letters B
Scopus coverage years: from 1996 to 2019
Publisher: World Scientific
ISSN: 0217-9849 E-ISSN: 1793-6640
Subject area:
Physics and Astronomy: Condensed Matter Physics
Physics and Astronomy: Statistical and Nonlinear Physics
View all documents
Set document alert
Save to source list
Journal Homepage
CiteScore 2018
0.85
SJR 2018
0.229
SNIP 2018
0.404
CiteScore
CiteScore rank & trend
CiteScore presets
Scopus content coverage
CiteScore 2018
Calculated using data from 30 April, 2019
0.85 = Citation Count 2018 / Documents 2015 - 2017* = 1 056 Citations / 1 239 Documents
*CiteScore includes all available document types
View CiteScore methodology
CiteScore FAQ
CiteScore rank
Category
Rank
Percentile
Physics and Astronomy
Condensed Matter Physics
#276/397
30th
Physics and Astronomy
Statistical and Nonlinear Physics
#31/43
27th
View CiteScore trends
Add CiteScore to your site
CiteScoreTracker 2019
Last updated on 08 December, 2019
Updated monthly
1.02 = Citation Count 2019 / Documents 2016 - 2018 = 1 464 Citations to date / 1 432 Documents to date
Metrics displaying this icon are compiled according to Snowball Metrics, a collaboration between industry and academia.

PREUVE D'INDEXATION DANS WEB OF SCIENCE

Return to Search Resu

MODERN PHYSICS LETTERS B

ISSN / eISSN **0217-9849 / 1793-6640**
Publisher **WORLD SCIENTIFIC PUBL CO PTE LTD, 5 TOH TUCK LINK, SINGAPORE, SINGAPORE, 596224**

General Information

Journal Website	Visit Site	**Publisher Website**	Visit Site
1st Year Published	1987	**Frequency**	Fortnightly
Issues Per Year	36	**Country / Region**	SINGAPORE
Primary Language	English	**Submission Website**	Visit Site

Some general information was sourced from the Directory of Open Access Journals and/or Transpose.

Web of Science Core Collection

Science Citation Index Expanded (SCIE)

Additional _Web of Science_ Indexes

Current Contents Physical, Chemical & Earth Sciences

Essential Science Indicators

Categories: Physics, Mathematical | Physics, Applied | Physics, Condensed Matter | Physics | Applied Physics/Condensed Matter/Materials Science

Log into *Web of Science* to discover research literature from this journal.

Journal Metrics

2018 Journal Impact Factor 0.929

Categories: Physics, Mathematical | Physics, Applied | Physics, Condensed Matter

PREUVE D'INDEXATION DANS MATHSCINET

Modern Physics Letters B. Condensed Matter Physics, Statistical Physics, Atomic, Molecular and Optical Physics

Journal Details

Abbreviation	Modern Phys. Lett. B
Publisher	World Sci. Publ.
Websites	worldscientific.com
ISSN (Print)	0217-9849
ISSN (Online)	1793-6640
Frequency	36 issues/vol./yr.
Publications Listed	1 258
Reference Lists	N/A
Publications Cited	161 (12,8% of publications)
Citations	349 from 309 publications
Latest Issue	2019, vol. 33, iss. 36
Earliest Issue	1987, vol. 1, iss. 5

Recent Issues

Volume	Issue	Year	
33	36	2019	View
33	35	2019	View
33	34	2019	View

List All Issues

Concise History

Title	Start	End
Modern Physics Letters B. Condensed Matter Physics, Statistical Physics, Atomic, Molecular and Optical Physics	1987	-

Journal Title History

AMERICAN MATHEMATICAL SOCIETY MATHSCINET MATHEMATICAL REVIEWS

Journal Title History

Modern Physics Letters B. Condensed Matter Physics, Statistical Physics, Atomic, Molecular and Optical Physics

1987 to 2019 - Modern Phys. Lett. B

Journal | Related | Issues

Title	Modern Physics Letters B. Condensed Matter Physics, Statistical Physics, Atomic, Molecular and Optical Physics
Abbreviation	Modern Phys. Lett. B
Publisher	World Sci. Publ.
ISSN (Print)	0217-9849
ISSN (Online)	1793-6640
Frequency	36 issues/vol./yr.

3- Tiré-à-part de l'article

Modern Physics Letters B
Vol. 32, No. 2 (2018) 1850015 (13 pages)

DOI: 10.1142/S021798491850015X

World Scientific
www.worldscientific.com

EFT study of critical properties of the mixed spin-2 and spin-$\frac{3}{2}$ Blume–Capel model on the honeycomb lattice

R. A. Yessoufou*,†,‡, M. Karimou* and F. Hontinfinde*,†

*Institute of Mathematics and Physical Sciences (IMSP), Republic of Benin

†Department of Physics, University of Abomey-Calavi, Republic of Benin

‡yesradca@yahoo.fr

Received 12 June 2017
Revised 4 September 2017
Accepted 12 October 2017
Published 11 January 2018

We use theoretical and numerical calculations in the framework of the effective-field theory to examine the rigorous effects of the crystal field interactions of the mixed spin-2 and spin-$\frac{3}{2}$ Blume–Capel model on the honeycomb lattice in the presence of an external magnetic field. The ground state phase diagram has been constructed. Thermal changes of the order parameters and other thermodynamic quantities of interest and their influence on the phase diagrams of the model have been thoroughly investigated. The system shows very interesting critical properties including continuous and discontinuous phase transitions, tricritical points and compensation temperatures which are revealed in specific ranges of the parameters space. Our numerical findings are compared to those obtained by other methods and reliable agreements are recovered.

Keywords: Critical phenomena; thermal changes; crystal fields interactions; mixed spin-2 and spin-$\frac{3}{2}$.

1. Introduction

Recently, in statistical and condensed matter physics, many extensive numerical investigations of various mixed spins Ising systems have been performed.[1–4] This increasing interest is due to the revelation of new and very important critical properties which cannot be detected during the study of their single-spin counterparts. The mixed spins Ising model has been one of the most used models to investigate ferrimagnetic materials in which numerous properties useful in modern technologies (ultra-high density magnetic storage and recording devices, biomedical applications etc.) are singled out.[5–10]

‡Corresponding author.

Theoretically, many authors used various numerical and computational methods to study these systems: effective-field theory,[11–20] mean-field approximation,[21–23] renormalization-group technique,[24] numerical simulations based on Monte Carlo[25–32] and recursion relations technique.[33–38] Albayrak,[38] by means of recursion relations technique, and Fathi[21] using the mean-field theory based on Bogoliubov inequality for the Gibbs free energy, studied the present model and found similar results and very interesting thermodynamic properties. Also, Deriven *et al.*[16] used the framework of EFT to investigate the Blume–Capel version of this model in the presence of a longitudinal magnetic field. More recently, Karimou *et al.*[34] studied the Blume–Emery–Griffiths version of the mixed spin-2 and spin-$\frac{3}{2}$ with equal crystal field in the presence of an applied magnetic field on the Bethe lattice by means of recursion relations technique and found very interesting results concerning the effects of the crystal field strengths, the biquadratic interaction and the magnetic field on the critical behaviors of the system.

In this work, we use the EFT to investigate the critical properties and finite temperature phase diagrams of the mixed spin-2 and spin-$\frac{3}{2}$ Blume–Capel system with unequal crystal fields on the honeycomb lattice in the presence of an external magnetic field. Our attention will be rigorously focused on the analysis of the critical contributions of the crystal fields and also the external magnetic field on the thermodynamic properties of the model. The present investigation is motivated in the sense that the synthesis of new magnetic materials which need to be extensively investigated for a good understanding of their ferrimagnetic properties is, nowadays, an active field of research in molecular magnetism. Mixed spins Ising models are an effective tool for such study.

The remaining part of this paper includes the following: in Sec. 2, the formulation of the model on the honeycomb lattice, calculations and analysis of its ground states phase diagram are covered. In Sec. 3, detailed numerical findings concerning the thermal behaviors of the order parameters, other thermodynamic quantities are deeply exposed and discussed. Finally in Sec. 4, we conclude.

2. Model and Its Ground States Calculations and Analysis

Let us consider the mixed spin-2 and spin-$\frac{3}{2}$ system composed of two interpenetrating sublattices A and B on the honeycomb lattice on which the model is formulated as shown in Fig. 1. The sites of sublattice A are covered by atoms of spins σ_i, where $\sigma_i = \pm 2, \pm 1, 0$. Those of the sublattice B are covered by atoms of spins S_j, where $S_j = \pm\frac{3}{2}, \pm\frac{1}{2}$. So, the Hamiltonian of such model with bilinear interaction parameter J ($J < 0$) between the nearest neighbor, the crystal field interactions D_A and D_B and the external magnetic field h acting on both sites of the system is given by

$$H = -J \sum_{\langle i,j \rangle} \sigma_i S_j - D_A \sum_i \sigma_i^2 - D_B \sum_j S_j^2 - h \left(\sum_j S_j + \sum_i \sigma_i \right). \qquad (1)$$

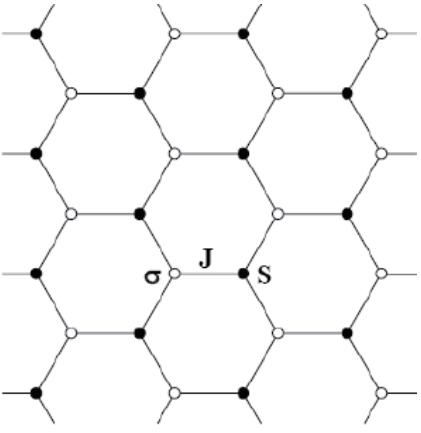

Fig. 1. The studied model composing of two interpenetrating sublattices A and B with spin variables $\sigma = 2$ and $S = \frac{3}{2}$, respectively, defined on the honeycomb lattice.

The first summation is carried out only over the nearest-neighbor pair of spins. Now, let us evaluate the mean values of $m_A = \langle \sigma_i \rangle$ and $m_B = \langle S_j \rangle$. For this, we make use of the exact Ising spin identities with the differential operator techniques introduced by Honmura and Kaneyoshi.[17,18] Thus, one can get the expressions of the two sublattices magnetizations as

$$\langle \sigma_i^l \rangle = \left\langle \prod_{\delta} [a_0(a) + a_1(a) S_{j+\delta} + a_2(a)(S_{j+\delta})^2 + a_3(a)(S_{j+\delta})^3] \right\rangle f_l(x)|_{x=0}\,, \tag{2}$$

$$\langle S_j^l \rangle = \left\langle \prod_{\delta} [b_0(a) + b_1(a)\sigma_{i+\delta} + b_2(a)(\sigma_{i+\delta})^2 + b_3(a)(\sigma_{i+\delta})^3 + b_4(a)(\sigma_{i+\delta})^4] \right\rangle g_l(x)|_{x=0}, \tag{3}$$

where δ and $a = J\nabla$ are, respectively, the coordination number and a new variable of the model which depends on the differential operator $\nabla = \frac{\partial}{\partial x}$. The function $f_l(x)$ and $g_l(x)$ are defined by

$$f_1(x) = \frac{4\sinh[2\beta(x+h)] + 2\sinh[\beta(x+h)]\exp(-3\beta D_A)}{2\cosh[2\beta(x+h)] + 2\cosh[\beta(x+h)]\exp(-3\beta D_A) + \exp(-4\beta D_A)}\,, \tag{4}$$

$$f_2(x) = \frac{8\cosh[2\beta(x+h)] + 2\cosh[\beta(x+h)]\exp(-3\beta D_A)}{2\cosh[2\beta(x+h)] + 2\cosh[\beta(x+h)]\exp(-3\beta D_A) + \exp(-4\beta D_A)}\,, \tag{5}$$

$$g_1(x) = \frac{3\sinh[\frac{3\beta}{2}(x+h)] + \sinh[\frac{\beta}{2}(x+h)]\exp(-2\beta D_B)}{2\cosh[\frac{3\beta}{2}(x+h)] + 2\cosh[\frac{\beta}{2}(x+h)]\exp(-2\beta D_B)}\,, \tag{6}$$

$$g_2(x) = \frac{9\cosh[\frac{3\beta}{2}(x+h)] + \cosh[\frac{\beta}{2}(x+h)]\exp(-2\beta D_B)}{2\cosh[\frac{3\beta}{2}(x+h)] + 2\cosh[\frac{\beta}{2}(x+h)]\exp(-2\beta D_B)}\,, \tag{7}$$

where $\beta = 1/k_B T$, k_B is the Boltzmann constant and T is the absolute temperature.

The coefficients $a_k(a)$ $(k = 0, \ldots, 3)$ for spin-$\frac{3}{2}$ and $b_m(a)$ $(m = 0, \ldots, 4)$ for spin-2 can be explicitly calculated by means of the exact van der Waerden identity as

$$\begin{aligned} a_0(a) &= \frac{1}{8}\left[9\cosh\left(\frac{a}{2}\right) - \cosh\left(\frac{3a}{2}\right)\right], \\ a_1(a) &= \frac{1}{12}\left[27\sinh\left(\frac{a}{2}\right) - \sinh\left(\frac{3a}{2}\right)\right], \\ a_2(a) &= \frac{1}{2}\left[-\cosh\left(\frac{a}{2}\right) + \cosh\left(\frac{3a}{2}\right)\right], \\ a_3(a) &= \frac{1}{3}\left[-3\sinh\left(\frac{a}{2}\right) + \sinh\left(\frac{3a}{2}\right)\right]. \end{aligned} \tag{8}$$

$$\begin{aligned} b_0(a) &= 1\,, \\ b_1(a) &= \frac{1}{6}[8\sinh(a) - \sinh(2a)]\,, \\ b_2(a) &= \frac{1}{12}[16\cosh(a) - \cosh(2a) - 15]\,, \\ b_3(a) &= \frac{1}{6}[-\sinh(a) + 2\sinh(2a)]\,, \\ b_4(a) &= \frac{1}{12}[-4\cosh(a) + \cosh(2a) + 3]\,. \end{aligned} \tag{9}$$

It is very important to mention that Eqs. (2) and (3) are exact and valid for all values of δ. If one tries to exactly treat all the spin–spin correlations for that set of equations, the problem rapidly seems intractable. So, a first obvious attempt to deal with is to neglect correlations and the decoupling approximations are expressed as

$$\begin{aligned} \langle\sigma_i(\sigma_{i'})^2\cdots(\sigma_{i^n})^4\rangle &\cong \langle\sigma_i\rangle\langle(\sigma_{i'})^2\rangle\cdots\langle(\sigma_{i^n})^4\rangle\,, \\ \langle S_j(S_{j'})^2(S_{j^n})^3\rangle &\cong \langle S_j\rangle\langle(S_{j'})^2\rangle\langle(S_{j^n})^3\rangle\,, \end{aligned} \tag{10}$$

where $i \neq i' \neq \cdots \neq i^n$ and $j \neq j' \neq \cdots \neq j^n$ have been introduced within the EFT with correlations.[17,18]

According to these approximations, one can reduce Eqs. (2) and (3) to

$$m_A = [a_0(a) + a_1(a)\langle S_j\rangle + a_2(a)\langle(S_j)^2\rangle + a_3(a)\langle(S_j)^3\rangle]^\delta f_1(x)|_{x=0}\,, \tag{11}$$

$$q_A = [a_0(a) + a_1(a)\langle S_j\rangle + a_2(a)\langle(S_j)^2\rangle + a_3(a)\langle(S_j)^3\rangle]^\delta f_2(x)|_{x=0}\,, \tag{12}$$

$$\begin{aligned} m_B = [&b_0(a) + b_1(a)\langle\sigma_i\rangle + b_2(a)\langle(\sigma_i)^2\rangle + b_3(a)\langle(\sigma_i)^3\rangle \\ &+ b_4(a)\langle(\sigma_i)^4\rangle]^\delta g_1(x)|_{x=0}\,, \end{aligned} \tag{13}$$

$$\begin{aligned} q_B = [&b_0(a) + b_1(a)\langle\sigma_i\rangle + b_2(a)\langle(\sigma_i)^2\rangle + b_3(a)\langle(\sigma_i)^3\rangle \\ &+ b_4(a)\langle(\sigma_i)^4\rangle]^\delta g_2(x)|_{x=0}\,. \end{aligned} \tag{14}$$

In the spirit to examine the thermal behaviors of the order parameters and then display different phase diagrams of interest, one can make use of Eqs. (11)–(14). After expanding the right-hand sides of Eqs. (11) and (13), one obtains the following set of coupled equations for the sublattice magnetizations:

$$\begin{aligned} m_A = {} & C_0 + C_1 m_B + C_2 m_B^2 + C_3 m_B^3 + C_4 m_B^4 + C_5 m_B^5 + C_6 m_B^6 \\ & + C_7 m_B^7 + C_8 m_B^8 + C_9 m_B^9 \,, \end{aligned} \tag{15}$$

$$\begin{aligned} m_B = {} & E_0 + E_1 m_A + E_2 m_A^2 + E_3 m_A^3 + E_4 m_A^4 + E_5 m_A^5 + E_6 m_A^6 \\ & + E_7 m_A^7 + E_8 m_A^8 + E_9 m_A^9 + E_{10} m_A^{10} + E_{11} m_A^{11} + E_{12} m_A^{12} \,, \end{aligned} \tag{16}$$

where the coefficients C_k $(k = 0, 1, \ldots, 9)$ and E_m $(m = 0, 1, 2, \ldots, 12)$ can be analytically calculated by applying the following mathematical relations: $\exp(\alpha\nabla) f(x)|_{x=0} = f(x+\alpha)|_{x=0}$ and $\exp(\alpha\nabla) g(x)|_{x=0} = g(x+\alpha)|_{x=0}$.

During our investigations, we also look for the compensation temperature which is located at the crossing point between the absolute values of the sublattice magnetizations m_A and m_B. For this, we thermally study the variations of the net or global magnetization m_T given by

$$m_T = \frac{m_A + m_B}{2} \,. \tag{17}$$

Also, for the investigation of the influences of the external magnetic field, we make use of the total susceptibility χ_T defined by

$$\chi_T = \left.\frac{\partial m_A}{\partial h}\right|_{h=0} + \left.\frac{\partial m_B}{\partial h}\right|_{h=0} . \tag{18}$$

Let us make a deep analysis of the ground state of the model in the absence of the external magnetic field. To determine the ground states, we need to express first from the Hamiltonian of Eq. (1) the contribution E_p of a pair of spins (σ, S) which is given by

$$E_p(\sigma, S) = \frac{J}{|J|}\sigma S - \frac{D_A}{\delta|J|}\sigma^2 - \frac{D_B}{\delta|J|}S^2 \,. \tag{19}$$

An interesting ground state phase diagram is obtained and illustrated in Fig. 2 after computing and comparing values of E_p for all possible configurations of the model. It follows from this figure that there are six stable phases denoted respectively by $O_1 \equiv (\pm 2, \mp\frac{3}{2}, 4, \frac{9}{4})$, $O_2 \equiv (\pm 2, \mp\frac{1}{2}, 4, \frac{1}{4})$, $O_3 \equiv (\pm 1, \mp\frac{3}{2}, 1, \frac{9}{4})$, $O_4 \equiv (\pm 1, \mp\frac{1}{2}, 1, \frac{1}{4})$, $D_1 \equiv (0, 0, 0, \frac{9}{4})$ and $D_2 \equiv (0, 0, 0, \frac{1}{4})$. The two last ones are two particular disordered phases where for example in the phase D_1 (respectively in the phase D_2), the sublattice magnetization $m_B = 0$ and the quadrupolar moment $q_B \neq 0$ because one-half of the sublattice is occupied by spin in state $\frac{3}{2}$ (respectively in state $\frac{1}{2}$) whereas the other half is occupied by spin in state $-\frac{3}{2}$ (respectively in state $-\frac{1}{2}$). Also, from this ground state phase diagram, other interesting and key features of the model can be identified. Among them, we have three multicritical points B_1, B_2 and B_3 where at least three phases coexist with eight coexistence lines. On some

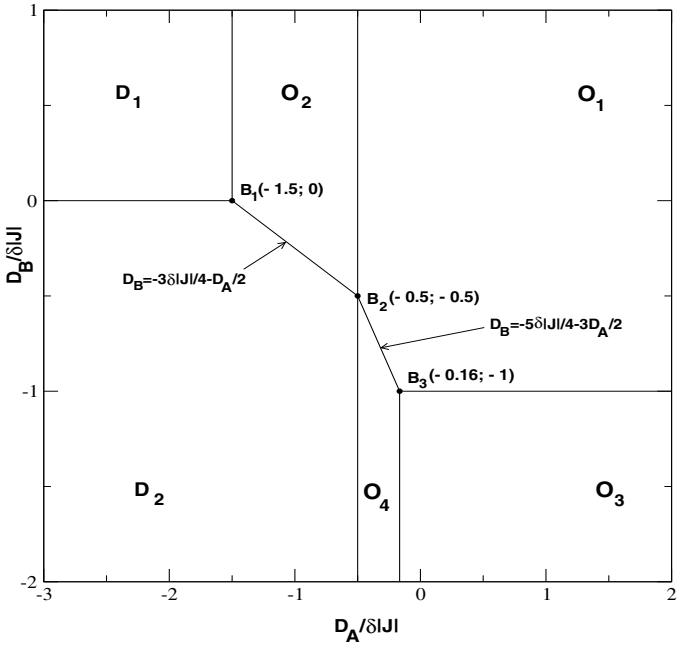

Fig. 2. Ground state phase diagram of the studied model in the $(D_A/\delta|J|, D_B/\delta|J|)$ plane (for more detailed description, see the text).

coexistence lines, we have some hybrid phases. For example, on the coexistence line between phases O_1 and O_2, one has the hybrid phase $(\pm 2, \mp 1, 4, 1)$. For large negative values of the two crystal fields, the dominant phase is the disordered phase D_1, whereas for large positive values of the two crystal fields, the dominant phase is the ordered phase O_1. Our ground state phase diagram is similar to the one displayed in Fig. 1 in Refs. 21, 22 and 38.

3. Numerical Findings and Discussions

In this section, we proceed to the exposition and the in-depth discussion of most results concerning the temperature dependence changes of the sublattice magnetizations, the global magnetization, the total susceptibility and the finite temperature phase diagrams.

3.1. *Thermal behaviors of the order parameters and the response function*

In order to characterize the nature of different transitions, identify the compensation phenomenon of the studied model and then illustrate different finite temperature phase diagrams of interest, we first study and analyze the thermal behaviors of the sublattice magnetizations m_A and m_B, the global magnetization m_T and the total susceptibility χ_T as depicted in Figs. 3 and 4. Figure 3(a) illustrates temperature

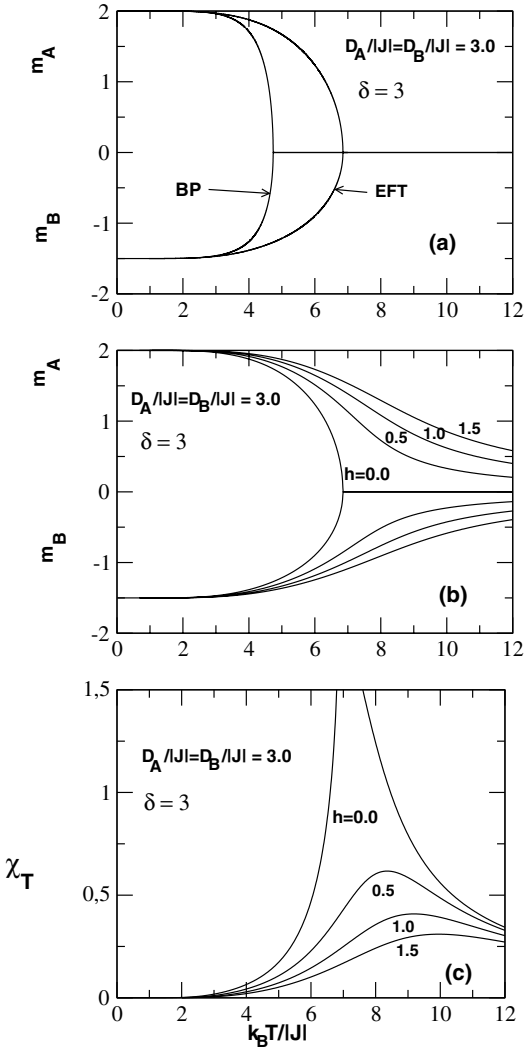

Fig. 3. Order parameters and response function as functions of the temperature when fixing $D_A/|J| = D_B/|J| = 3$. Panel (a): thermal variations of the sublattice magnetizations m_A and m_B for two different methods. Panels (b–c): thermal variations of the sublattice magnetizations m_A, m_B and the total susceptibility χ_T for four values of the magnetic field as indicated in the figure.

dependences of the sublattice magnetizations for two different methods: the Bethe Peierls approach (BP) and the EFT. From this figure, it emerges that the two sublattice magnetizations continuously decrease from their saturation values $m_A = 2$ and $m_B = -\frac{3}{2}$ at $T = 0$ to zero at T_c as the temperature increases. Numerical calculations indicate that the second-order phase transition occurs at $T_c/|J| = 6.923$ for (EFT) and $T_c/|J| = 4.773$ for (BP). The phase transition is from the ordered

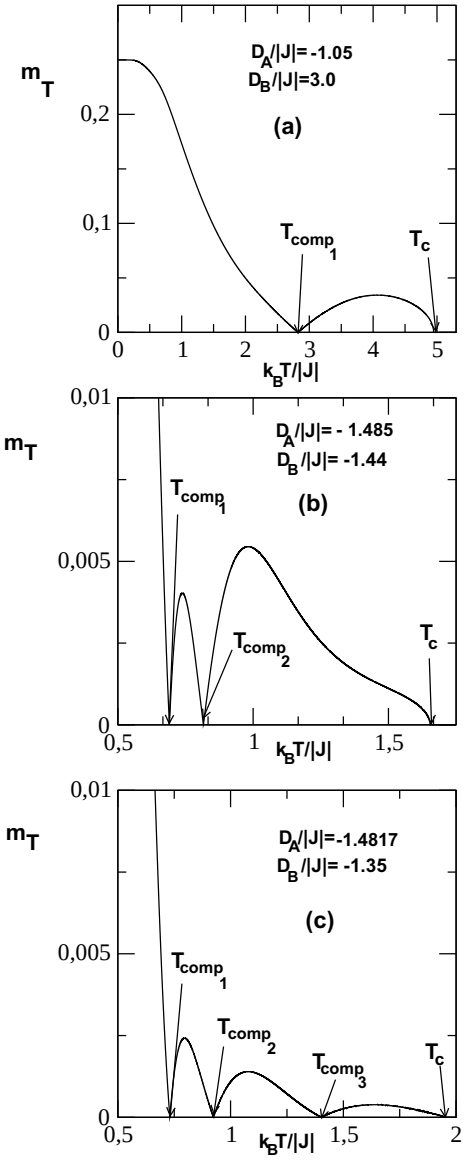

Fig. 4. Total magnetization m_T as a function of the temperature for several selected values of crystal fields $D_A/|J|$ and $D_B/|J|$ as indicated in different panels of the figure. The model shows one, two or three compensation temperatures which strongly depend on values of the two crystal fields, especially for the negative ones.

ferrimagnetic phase O_1 to the paramagnetic phase (P). One can remark that the phase transition temperatures T_c are not the same for both methods and this appears normal. Also, the (EFT) seems to more overestimate the phase transition temperature of the model. Figures 3(b) and 3(c) show thermal behaviors of sub-

lattice magnetizations and the total susceptibility as functions of the temperature for four values of the magnetic field $h/|J|$ when $D_A/|J| = D_B/|J| = 3$. From panel (b) to panel (c), one notes what follows. First, the sublattice magnetizations after their decrease do not go to zero for $h/|J| \neq 0$. This means that the model does not show transition for $h/|J| \neq 0$. Also, the absolute remaining values of the sublattice magnetizations increase as the magnetic field strength increases. Second, it is clear that the global susceptibility χ_T diverges at T_c for $h/|J| = 0$, but for $h/|J| \neq 0$, it shows a maximum and by increasing the magnetic field value, the height of the maximum decreases, whereas the temperature value at which this maximum appears increases. So, one can conclude that the magnetic field really affects the magnetic properties of the model.

Now, let us pay some attention to the compensation phenomenon in the model. For this, we plotted in Fig. 4 thermal variations of the global magnetization m_T as a function of the temperature for selected values of the two crystal fields. From this figure, it follows that the model exhibits the compensation phenomenon. Indeed, one can observe from different panels of the figure that the system presents one, two and three compensation temperatures which strongly depend on the values of the two different crystal fields. It is important to mention that the selected negative values of the two applied crystal fields favor more the appearance of two or three compensation points. Figure 4 shows same topologies as Fig. 5 of Ref. 21.

3.2. *Phase diagrams of the model*

In order to provide a deeper insight into how the two different crystal fields affect the overall critical phenomena of the studied model, we plotted in Figs. 5–7 different phase diagrams in the form of critical temperature as a function of both crystal field strengths in zero magnetic field. In these figures, solid, dashed, dotted lines and black triangles, respectively, indicate the second-, first-order phase transitions, compensation lines and tricritical points. In the following, first-order transitions are obtained when jump discontinuities appear in the thermal variations of calculated order parameters and magnetic susceptibilities.

The first phase diagram is obtained in the $(D_B/|J|, kT_c/|J|)$ plane for several selected values of $D_A/|J|$ as shown in Fig. 5. From this figure for $D_A/|J| > -\frac{3}{2}$, the phase transition lines are all of second-order separating the order ferrimagnetic phase (F) from the paramagnetic phase (P). All of them present different constant critical temperatures as $D_B/|J| \to -\infty$. Especially for $D_A/|J| \geq 6$, the second-order transition lines show the same critical temperature $kT_c/|J| = 3.079$ for large negative values of $D_B/|J|$. Also, for $D_A/|J| = -\frac{3}{2}$, the phase transition line is of the second-order. For $-4 < D_A/|J| < -\frac{3}{2}$, the transition line behaviors drastically change and the model exhibits a tricritical behavior, i.e. the occurrence of tricritical points where second-order phase transition lines and the first-order ones are connected. In this domain, as $D_A/|J|$ decreases, the portion of the first-order transition line increases. For $D_A/|J| \leq -4$, all the phase transition lines are of first-order

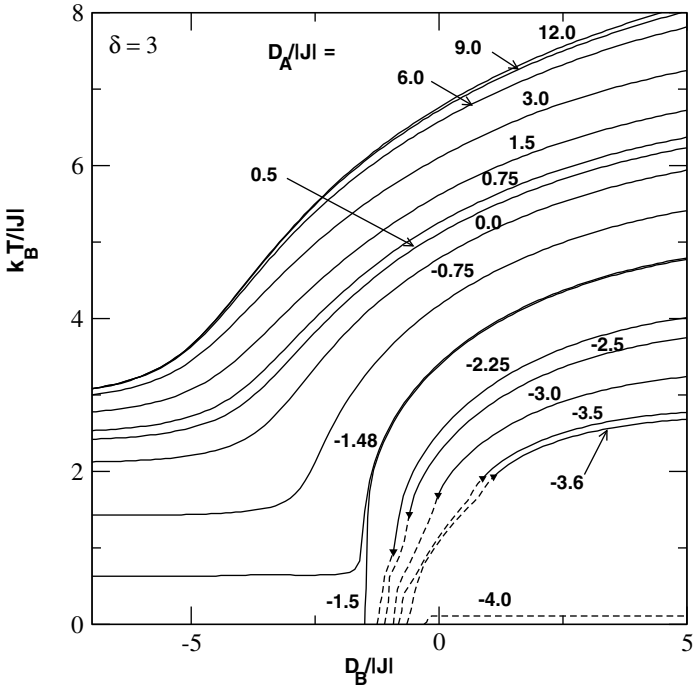

Fig. 5. Phase diagram in the $(D_B/|J|, k_BT/|J|)$ plane for several values of $D_A/|J|$. The lines are labeled with the values of $D_A/|J|$. Solid, dashed lines and black triangles, respectively, indicate the second-order, first-order transition lines and the tricritical points. It is important to mention that the same representation is also valid for the rest phase diagrams. For $D_A/|J| > -\frac{3}{2}$, the system shows constant temperature values at large negative values of $D_B/|J|$ and all the phase transition lines are of second-order.

kind. So, as the second-order phase transition disappears, only the first-order phase transition dominates. This phase diagram shows some similarities with Fig. 2(a) of Ref. 22, Fig. 3 of Ref. 38 and Fig. 2 of Ref. 21.

The second phase diagram is calculated in $(D_A/|J|, kT_c/|J|)$ plane for various selected values of $D_B/|J|$ as it is seen in Fig. 6. This figure also expresses interesting properties of the model. Indeed, for all values of $D_B/|J|$, the second-order phase transition line is connected to the first-order phase transition line which is obtained at low temperature at a tricritical point. So, for $D_B/|J| \leq -\frac{3}{2}$, a unique tricritical point at which all the second-order phase transition lines are connected to the corresponding first-order transition ones is given by $(D_A/|J| = -1.444, kT_c/|J| = 0.501)$. A same result is obtained for $D_B/|J| \geq 3$ and the tricritical point here is given by $(D_A/|J| = -4.211, kT_c/|J| = 1.244)$. Figure 6 bears some resemblances with Figs. 4(a) and 4(c) of Ref. 38, and also with Fig. 2 of Ref. 22 and Fig. 3 of Ref. 21.

In the same way as it is done for the second phase diagram, we displayed in Fig. 7 the compensation lines of the model. Indeed, one remarks that for $D_B/|J| \geq -1.26$,

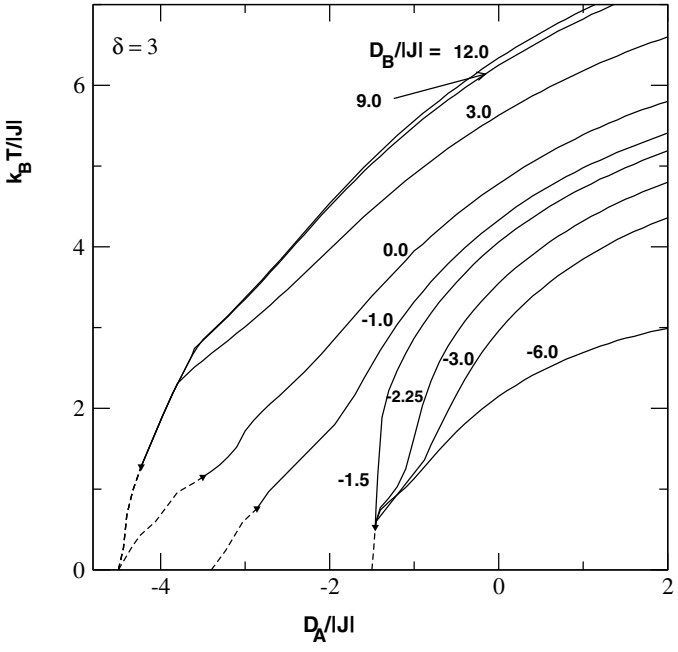

Fig. 6. Phase diagram in the $(D_A/|J|, k_BT/|J|)$ plane for various values of $D_B/|J|$. The lines are labeled with the values of $D_B/|J|$. The system presents a tricritical behavior for all values of $D_B/|J|$. Especially for $D_B/|J| \geq 3$ (respectively for $D_B/|J| \leq -\frac{3}{2}$), the system exhibits a unique tricritical point, respectively.

the model only exhibits one compensation temperature, whereas for $D_B/|J| < -1.26$ and in a specific range of negative values of $D_A/|J|$, the system shows two or three compensation temperatures. All these findings are in perfect agreement with Fig. 4 of Ref. 21 and Fig. 4(b) of Ref. 38.

4. Conclusion

In this paper, via the framework of the effective-field theory, we single out the effects of the interaction parameters on the critical behaviors and phase diagrams of the mixed spin-2 and spin-$\frac{3}{2}$ Blume–Capel system with unequal single-ion anisotropies on the honeycomb lattice in the presence of an external magnetic field.

First, we have investigated as shown in Fig. 2 the ground state phase diagram which is very useful for a good classification of regions of different stable states and for a reliable checking in the construction of the finite temperature phase diagrams at very low temperatures. Also, in Figs. 3 and 4, the thermal variations of the sublattice magnetizations, the total magnetization and the total susceptibility are rigorously investigated in order to find the nature (continuous or discontinuous) of the phase transitions, as well as calculate the compensation points. Then as it is seen in Figs. 5–7, different finite temperature phase diagrams are displayed

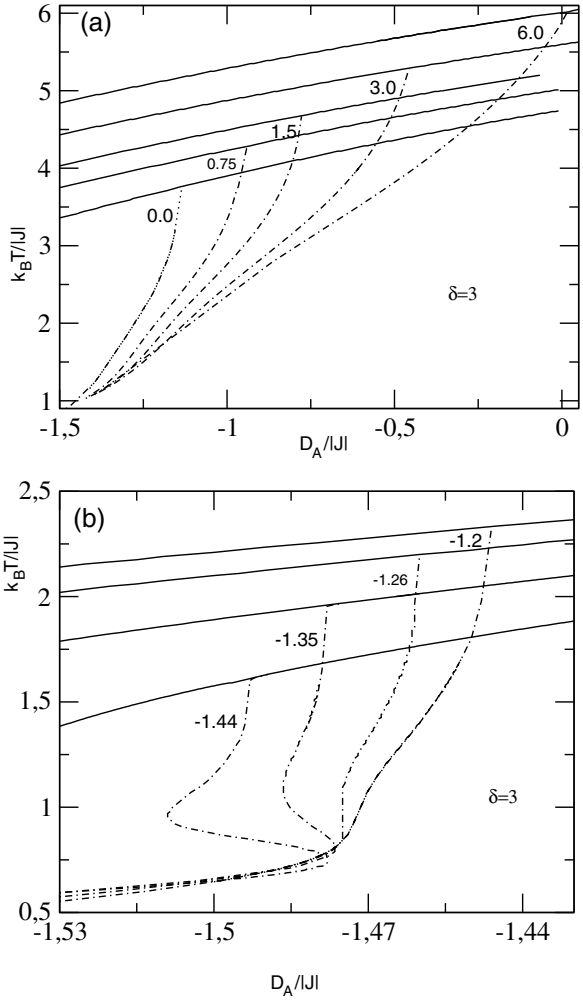

Fig. 7. Compensation temperatures (dotted lines) as functions of $D_A/|J|$ for various values of $D_B/|J|$. The lines are labeled with the values of $D_B/|J|$. The system presents one, two or three compensation temperatures in specific ranges of values of the crystal fields interactions, especially the negative ones.

in all planes of interest in zero external magnetic field. We have found that the model revealed interesting ferrimagnetic properties such as the first- and second-order phase transitions, tricritical points and compensation temperatures which are all strongly dependant on the competition between interaction parameters of the model, especially the two different crystal fields interactions.

By comparing our findings with those of Refs. 21, 22 and 38, reliable agreements are found. It is very important to indicate that our results are more interesting than those found in Ref. 16 where authors used the same method to study the present model but with equal crystal field strength in the presence of a magnetic field.

References

1. R. M. White, *Science* **229** (1985) 11.
2. R. Wood, *Understanding Magnetism* (Tab Books Inc., PA, 1988).
3. E. Köster, *J. Magn. Magn. Mater.* **120** (1988) 1.
4. L. B. Lueck and R. G. Gilson, *J. Magn. Magn. Mater.* **88** (1999) 227.
5. K. Itoh and M. Kinoshita, *Molecular Magnetism: New Magnetic Materials* (Kodansha, Tokyo, 2000).
6. W. Linert and M. Verdaguer (eds.), *Molecular Magnets: Recent Highlights* (Springer, Berlin, 2003).
7. D. Gatteschi, *Adv. Mater.* **6** (1994) 635.
8. J. S. Miller and A. J. Epstein, *Chem. Eng. News* **73** (1995) 30.
9. O. Kahn, *Molecular Magnetism* (VCH, New York, 1993).
10. A. Bobák, *Physica A* **258** (1998) 140.
11. T. Kaneyoshi, *J. Phys. Soc. Jpn.* **56** (1987) 2675.
12. T. Kaneyoshi, *Physica A* **153** (1988) 556.
13. T. Kaneyoshi, *J. Magn. Magn. Mater.* **92** (1990) 59.
14. A. Benyoussef, A. El Kenz and T. Kaneyoshi, *J. Magn. Magn. Mater.* **131** (1994) 173.
15. A. Benyoussef, A. El Kenz and T. Kaneyoshi, *J. Magn. Magn. Mater.* **131** (1994) 179.
16. B. Deviren, E. Kantar and M. Keskin, *J. Korean Phys. Soc.* **56** (2010) 1738.
17. R. Honmura and T. Kaneyoshi, *J. Phys. C: Solid State Phys.* **12** (1979) 3979.
18. T. Kaneyoshi and H. Beyer, *J. Phys. Soc. Jpn.* **49** (1980) 1306.
19. T. Kaneyoshi, *Physica A* **205** (1994) 677.
20. D. F. de Albuquerque, S. R. L. Alves and A. S. de Arruda, *Phys. Lett. A* **346** (2005) 128.
21. A. Fathi, *Open J. Appl. Sci.* **3** (2013) 218.
22. H. Miao, G. Wei and J. Geng, *J. Magn. Magn. Mater.* **321** (2009) 4139.
23. W. G. Zhu and M. H. Ling, *Commun. Theor. Phys.* **51** (2009) 756.
24. S. G. A. Quadros and S. R. Salinas, *Physica A* **206** (1994) 479.
25. G. M. Zhang and C. Z. Yang, *Phys. Rev. B* **48** (1993) 9452.
26. G. M. Buendia and M. A. Novotny, *J. Phys.: Condens. Matter* **9** (1997) 5951.
27. M. Godoy and W. Figueiredo, *Phys. Rev. E* **65** (2002) 026111.
28. M. Godoy and W. Figueiredo, *Phys. Rev. E* **66** (2002) 036131.
29. G. Wei, Q. Zhang and Y. Gu, *J. Magn. Magn. Mater.* **301** (2006) 245.
30. G. Wei, Y. Gu and Jing Liu, *Phys. Rev. B* **74** (2006) 024422.
31. M. Zukovič and A. Bobák, *Physica A* **389** (2010) 5401.
32. M. Zukovič and A. Bobák, *J. Magn. Magn. Mater.* **322** (2010) 2868.
33. R. A. Yessoufou, S. Bekhechi and F. Hontinfinde, *Eur. Phys. J. B* **81** (2011) 137.
34. M. Karimou, R. Yessoufou and F. Hontinfinde, *World J. Condens. Matter Phys.* **5** (2015) 187.
35. E. Albayrak and A. Yigit, *Chinese Phys. B* **21** (2012) 020511.
36. M. Karimou, R. A. Yessoufou, T. D. Oké, A. Kpadonou and F. Hontinfinde, *Condens. Matter Phys.* **19** (2016) 33003-1.
37. E. Albayrak, *Int. J. Mod. Phys. B* **17** (2008) 1087.
38. E. Albayrak, *Physica B* **391** (2007) 47.